Discovery of Inhibitors of MicroRNA-21 Processing Using Small Molecule Microarrays

Colleen M. Connelly[†], **Robert E. Boer**[†], **Michelle H. Moon**[†], **Peter Gareiss**[‡], and **John S. Schneekloth Jr.**[*,†]

[†]Chemical Biology Laboratory, National Cancer Institute, Frederick, Maryland 21702, United States

[‡]Yale Center for Molecular Discovery, West Haven, Connecticut 06516, United States

Abstract

The identification of small molecules that bind to and perturb the function of microRNAs is an attractive approach for the treatment for microRNA-associated pathologies. However, there are only a few small molecules known to interact directly with microRNAs. Here, we report the use of a small molecule microarray (SMM) screening approach to identify low molecular weight compounds that directly bind to a pre-miR-21 hairpin. Compounds identified using this approach exhibit good affinity for the RNA (ranging from 0.8–2.0 μM) and are not composed of a polycationic scaffold. Several of the highest affinity compounds inhibit Dicer-mediated processing, while in-line probing experiments indicate that the compounds bind to the apical loop of the hairpin, proximal to the Dicer site. This work provides evidence that small molecules can be developed to bind directly to and inhibit miR-21.

Graphical Abstract
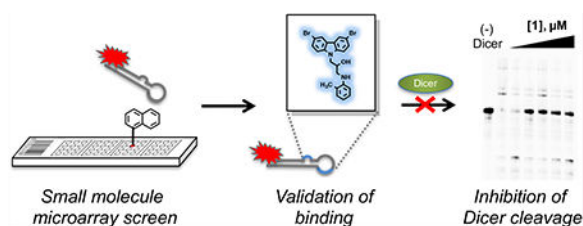
The goal of developing RNA-binding small molecule therapeutics is an area of increasing interest.[1–4] However, the discovery of molecules that bind to RNA with good affinity and specificity is a major challenge. RNA is a highly polar molecule with a flexible, dynamic structure and largely solvent-exposed binding pockets that are structurally distinct from

---

small molecule binding sites on proteins. While historically molecules like aminoglycosides have been studied as RNA binders, these compounds suffer from poor specificity and systemic toxicity. Therefore, approaches that identify small molecules with new RNA-binding chemotypes are needed. Furthermore, recent discoveries of novel classes of noncoding, regulatory RNAs[5] have provided substantial evidence for a variety of roles for RNA in cancer.[6–8]

One such class of noncoding RNAs is the family of microRNAs (miRNAs), ~22 nucleotide sequences produced by Drosha and Dicer processing of longer RNA hairpins. MiRNAs suppress gene expression by binding to partially complementary sequences in target mRNAs leading to either cleavage of the mRNA by the RNA-induced Silencing Complex (RISC) or inhibition of translation.[9] Aberrant expression of these regulatory miRNAs has been implicated in the development, metastasis, and progression of a wide range of human cancers as well as other diseases including cardiovascular disease and immune disorders.

A powerful example of a disease-associated miRNA is miR-21,[10,11] the overexpression of which has been observed in many human cancers including glioblastomas, lymphomas, breast, pancreatic, cervical, colorectal, ovarian, liver, and lung cancers. The overexpression of miR-21 in various tumors leads to reduced levels of miR-21 targets *in vivo*, many of which are tumor suppressors.[12] Knockdown of miR-21 with antisense agents induces apoptosis in glioblastoma,[13,14] breast cancer,[15] and hepatocellular carcinoma cell lines.[16,17] Further, a direct relationship between miR-21 overexpression and pre-B-cell lymphoma development has been demonstrated in a mouse model, providing evidence for miR-21 as a potential therapeutic target.[12]

The identification of small molecules that bind to "oncomiRs" such as miR-21 could provide a viable approach for the inhibition of miRNAs involved in cancer development and could lead to mechanistically new cancer therapies. Small molecules that inhibit the cellular function of miR-21 have been discovered; however, the mechanism of action of these inhibitors has not been elucidated, and they do not appear to bind directly to the RNA.[18,19] Similarly, aminoglycoside,[20] peptide/protein,[21] and peptoid-based[22,23] inhibitors of miR-21 have been studied. A long-standing goal has been to develop small molecules that directly bind to miR-21 in order to inhibit its biogenesis and function, and to date, this has proven challenging, with only a small number of compounds reported.[20,22,23]

Here, we employ a small molecule microarray (SMM) screen of a large library of druglike molecules to identify new motifs that bind to the pre-miR-21 hairpin. Hit compounds that showed selective binding to miR-21 over other oligonucleotides were validated through a series of biochemical and biophysical experiments. Through synthesis and analysis of a focused library, we demonstrate that this series of compounds exhibits a clear structure–activity relationship. Multiple affinity measurements show that several compounds display low micromolar to high nanomolar binding to the RNA hairpin. Dicer processing and in-line probing experiments further demonstrate that the compounds bind near the apical loop of the hairpin and inhibit formation of the mature miRNA. The compounds described here provide evidence that small molecules that bind directly to miR-21 can be used to block miRNA biogenesis and serve as miR-21 inhibitors.

RESULTS AND DISCUSSION

SMMs are a powerful tool for the high throughput screening of compound libraries against biological targets of interest[24–29] and have successfully been used to identify druglike small molecules that bind to nucleic acid targets including both DNA[30] and RNA.[31] Briefly, in this technique, small molecules are spatially arrayed and covalently linked to a functionalized glass surface using a robotic microarrayer. Slides are then hybridized with a fluorescently labeled oligonucleotide and imaged. Array features that increase in fluorescence indicate binding to the oligonucleotide (Figure 1A). To identify small molecules that bind to miR-21, we performed an SMM screen with a fluorescently labeled pre-miR-21 hairpin. A 29-mer RNA hairpin was designed containing the pre-miR-21 Dicer cleavage site and was labeled with a Cy5 fluorophore at the 5′ end (Figure 1B). SMM slides were incubated with the hairpin at a concentration of 500 nM for 1 h, after which slides were washed and imaged using a previously reported protocol.[30,31] In parallel, an identical screen was performed using the HIV Transactivaiton Response (TAR) RNA hairpin to control for selectivity in binding. Next, data analysis was performed to generate a composite Z-score for each compound in the library, and compounds with a Z-score > 3 were considered hits. In total, a library of 20 000 compounds was screened, and 19 compounds were identified as binding to the miR-21 hairpin but not the TAR hairpin for a hit rate of 0.1%.

From the 19 hit compounds that were identified in the SMM screen, 11 were selected for further analysis and purchased from commercial vendors (Figure S1). Of note, in the set of 19 total hits, seven of these compounds contained a common chemotype. Thus, only the highest scoring members of this group of compounds were purchased for initial follow-up analysis. To evaluate the binding of hit compounds to miR-21, a series of biochemical assays and affinity measurements were performed (Figure 2). Initially, each hit compound was analyzed in a differential scanning fluorimetry (DSF) assay, where the melting temperature (T_m) of the RNA was measured in the presence and absence of each compound. Changes in the T_m of the hairpin indicate compound interaction with the RNA. Of the 11 compounds, **1** and **2** (Figure 1C) showed reproducible T_m values of −5.1 ± 1.9 and −2.3 ± 0.3 °C, respectively, indicating binding to the hairpin. These compounds were among the highest scoring hits from the SMM screen and showed selectivity for miR-21 over the TAR hairpin, and their chemotype was represented in multiple screening hits. Therefore, these two compounds were selected for further analysis.

The DSF analysis provides reliable qualitative evidence for compound binding but is not used to measure equilibrium dissociation constant (K_d) values. To establish K_d values for each compound, we utilized two orthogonal fluorescence titration assays. First, each compound was titrated into a solution containing a 2-aminopurine-labeled (2-AP) RNA hairpin, where A15 was replaced with 2-AP.[23] Compound-induced changes in 2-AP fluorescence are used to derive a K_d value. In parallel, a fluorescence intensity assay (FIA) was performed. Compounds were titrated into a solution containing the Cy5-labeled hairpin used in the SMM screen, and changes in fluorescence intensity were measured by fluorescence spectroscopy and fit to a binding curve. In the 2-AP assay, compounds **1** and **2** were found to have K_d values of 2.3 ± 0.5 μM and 0.8 ± 0.2 μM, respectively. Similarly, when measured by FIA, **1** and **2** had K_d values of 3.2 ± 0.7 μM and 0.7 ± 0.1 μM,

respectively. Affinity measurements in the presence of excess yeast tRNA were unaffected, indicating a specific binding interaction (Supporting Figure S2). The K_d values were in good agreement between the two assays, despite different fluorophores and conditions, suggesting that both assays are faithfully reporting on compound affinity measurements and would be valid for evaluating binding.

To evaluate the structure–activity relationship (SAR) of compounds **1** and **2**, we assembled a library of synthetic and commercially available analogs. We used an efficient synthetic route that would enable rapid access to a variety of compounds differing in the substitution patterns throughout the core scaffold.[32,33] Beginning with commercially available 3,6-dibromocarbazole, alkylation with epichlorohydrin produced an epoxide,[34] which could be readily opened with substituted anilines or other nitrogen heterocycles in a BiCl$_3$-catalyzed reaction. This approach was used to generate a series of analogs (**3–9**) differing in aromatic ring substitution patterns (Table 1). Nine commercially available analogs in this series were purchased as well (**10–16**, Table 1), several of which were also identified as hits in the SMM screen. In addition to changing the aniline-containing functionality, we evaluated perturbations to the carbazole moiety (Table 2) as well as the linker structure and length (Table S1). To generate analogs satisfying these criteria, we modified the synthetic route to accommodate differentially substituted carbazoles (**17–23**), bromoindoles (**24**), diarylamines (**25–27**), and different linkers (**SI10–12**).[35] In total, we assembled a library of 30 analogs, including substitutions and modifications on almost all sites of the active structure.

Once the library was complete, each compound was evaluated in the DSF, FIA, and 2-AP assays to compare binding affinity for the miR-21 hairpin (Tables 1, 2, S1). In general, the K_d values from both FIA and 2-AP assays showed good agreement. Additionally, most compounds that showed good affinity exhibited larger T_m in the DSF assay. Alteration of the aniline substituent (**3–16**) was permissive, with most analogs displaying comparable binding affinity. Here, the best performing compounds contained a simple aromatic ring with a single alkoxy, halo, or alkyl substituent. Presumably, this class of compounds is conjugated to the SMM surface *via* reaction with the aniline nitrogen (or the neighboring secondary alcohol). These groups would thus be near the surface of the array and are not likely to be involved in direct contact with the RNA. The largest changes occurred with perturbation of the carbazole core, where removal of the bromide substituents (**17**), removal of one of the arenes (**24**), or replacement of the carbazole with a diarylamine (**25–27**), resulted in compounds with dramatically reduced binding. Changing the substitution pattern of the halides on the carbazole (**18–22**) had a more modest effect, as did changing bromo- to chloro- substitution (**23**). Alterations to the linker between the carbazole and aniline substituents also had modest effects, with longer linker lengths or modification of the secondary alcohol being associated with slightly weaker binding (Table S1, **SI10–12**). The most active compounds in the series had K_d values of ~1–3 μM with large effects in the DSF assay (T_m = −5 to −9 °C). Taken together, these data indicate an SAR whereby the dibromocarbazole functionality is important for interaction with the RNA, while linker length and aniline substitution effects are less impactful.

On the basis of their relatively high affinities for the miR-21 hairpin, six compounds were assessed for their ability to repress the levels of mature miR-21 through inhibition of Dicer-

mediated maturation of the pre-miRNA.[22] As validated by the DSF and fluorescence intensity assays, the small molecules bind to the truncated miR-21 hairpin, which contains many but not all of the secondary structural elements found in the wild type pre-miR-21 RNA. Binding of small molecules to the pre-miR-21 hairpin could inhibit the ability of Dicer to recognize and efficiently process pre-miR-21, thus inhibiting mature miR-21 biogenesis. To test this hypothesis, a Dicer cleavage assay was performed on a full length 60 nt 5′-AlexaFluor 647-labeled premiR-21 hairpin (Figure 1B). This hairpin was completely cleaved by Dicer to produce a 22-nt fragment consistent with mature miR-21 formation. The consumption of pre-miR-21 substrate was observed by in-gel fluorescence. A dose-dependent inhibition of Dicer cleavage was observed upon treatment of pre-miR-21 with increasing concentrations of the initial SMM hit compound **1** (Figure 3A). Here, inhibition of Dicer processing occurred at concentrations near the K_d values observed in affinity titration experiments. Preincubation of the RNA with each of six related carbazole derivatives at a concentration of 1 μM led to a significant inhibition of Dicer-mediated cleavage and an increase in the quantity of full length pre-miR-21 after ribonuclease treatment (Figure 3B). Compounds **1** and **2**, initially identified in the SMM screen, displayed 47% and 59% inhibition, respectively. Notably, treatment with analogs **6**, **7**, **11**, or **13** produced levels of full length pre-miR-21 that were equal to that of control reactions performed in the absence of Dicer. Thus, Dicer cleavage was abrogated upon compound binding. These results suggest that compound binding to the RNA may either physically block Dicer access to the pre-miRNA or induce structural changes that impair the efficiency of Dicer processing of the premiRNA.

To gain insight into the region of binding of the small molecules to the miR-21 hairpin, a Mg^{2+} induced in-line probing assay[36] was performed with **13** and the 5′-Cy5-labeled miR-21-hp used in the SMM screen.[22,23] The 5′-Cy5-labeled miR-21 hairpin (3 μM) was incubated with or without **13** at increasing concentration (3–300 μM) in buffer containing 1 mM $MgCl_2$ for 4 days. A previously reported miR-21-binding aminoglycoside, streptomycin, was used as a positive control for binding.[20] The resulting cleavage products were separated by PAGE, visualized by in gel fluorescence, and quantified to assess the cleavage efficiency across the various conditions (Figure 4A). In the absence of a small molecule, Mg^{2+} induced in-line cleavage predominately in the apical loop, with lower efficiency in the base-paired region. When the miR-21 hairpin was analyzed in the presence of **13**, the resulting cleavage pattern was markedly different from that generated in the absence of ligand, suggesting that compound binding affects the conformation or flexibility of the RNA within those regions. Notably, cleavage after residues C17, U18, and C19 in and near the apical loop was significantly reduced with increasing concentration of **13** (Figure 4A and B). Similarly, reductions in reactivity after U11 and U12, located in and near a single nucleotide bulge proximal to the apical loop, were also observed. Changes were observed in multiple experiments, and a representative experiment is shown in Figure 4A. Consistent with the literature reported binding site determined by S1 nuclease probing, treatment with a known miR-21-binding aminoglycoside, streptomycin, also led to a reduction in cleavage after positions C17, U18, and C19. In order to quantitate differences in cleavage patterns, replicate experiments were analyzed in triplicate at three concentrations. Here, the most marked and consistent decreases in reactivity were also observed after C17, U18, and C19

(Figure S3). These compound-induced changes in cleavage patterns indicate binding of **13** to the miR-21 hairpin proximal to or within the apical loop region (Figure 4C).

The identification of small molecules that bind directly to miR-21 has proven challenging to date. In this work, we demonstrate that a SMM screening approach can be used to identify molecules that bind to miR-21 and inhibit the processing of the pre-miR-21 hairpin by Dicer. Molecules within this series display a clear structure–activity relationship. More specifically, the dibromocarbazole functionality of the molecule appears to play a key role in promoting the interaction of the compounds with the hairpin. Modification of linker length or composition provided modest changes, as did alteration of the aniline substituents. The best compounds in this series, such as **2** and **13**, displayed 0.8–2.0 μM equilibrium dissociation constants as measured by both 2-AP and FIA affinity measurements. When evaluated by DSF, these compounds uniformly caused a decrease in the melting temperature of the 29-mer miR-21-hp RNA. This is in contrast to most binding interactions, which increase T_m, and indicates that the compounds destabilize the hairpin structure upon binding. Several compounds within this series also displayed inhibitory activity in a Dicer-mediated nuclease cleavage assay, indicating that they interfere with mature miR-21 biogenesis. In-line probing analysis of **13** demonstrates that C17, U18, C19, U11, and U12 are protected from cleavage upon compound incubation, providing evidence that the compounds interact with the hairpin at or near the apical loop. Thus, the compounds may be blocking Dicer-mediated hairpin processing by binding near the apical loop proximal to the Dicer site.

Taken together, the data presented here suggest that the longstanding goal of inhibiting miR-21 biogenesis using a small molecule inhibitor may in fact be possible. The chemical structure of the inhibitors described in this manuscript is distinct from the aminoglycoside, peptoid, or peptide-based miR-21-binding inhibitors previously reported. The reported structures stand as relatively rare examples of nonaminoglyco-side small molecules that bind to miR-21. Molecules similar to **1** and **2** have previously been studied in other contexts. For example, P7C3 (**10**) and derivatives have been studied extensively as proneurogenic compounds *in vivo* and have been shown to have good bioavailability.[32,33,37] P7C3 appears to exert neuroprotective effects by binding nicotinamide phosphoribosyltransferase (NAMPT), an enzyme involved in NAD salvage.[38] Thus, molecules in this series may interact with RNA molecules as well as proteins. However, the interaction between P7C3 derivatives and RNA has not been explored previously. Notably, a highly neuroprotective fluoro derivative of P7C3 (**SI12**) is less active than other derivatives in miR-21 binding assays, highlighting differences in SAR between RNA binding and pro-neurogenic activity. Given that the compounds reported here have established SAR, selectivity, and *in vitro* potency against a molecular target, this work can be considered a first step toward developing a chemical probe for miR-21.[39]

In summary, we have reported the discovery of a small molecule that binds to miR-21 and inhibits the maturation of the microRNA hairpin by binding near the apical loop and preventing Dicer processing. An SMM screening approach was key to the rapid identification of lead structures, which display good binding affinity for the RNA in multiple biophysical assays. Future efforts will focus on the development of more potent and selective analogs capable of blocking miR-21 biogenesis in cellular models, which would

demonstrate a fundamentally novel approach for the treatment of a broad variety of cancers. Finally, this work highlights the potential of SMM screening approaches for future efforts toward identifying druglike small molecule inhibitors of other disease-associated RNAs.

MATERIALS AND METHODS

General RNA Information.

To avoid RNase contamination, all buffers were prepared with DEPC-treated water, and all surfaces and equipment were decontaminated with RNaseZap (Ambion) prior to RNA handling. Deprotected and HPLC purified oligonucleotides were purchased from Dharmacon (ThermoFisher) or IDT DNA with the following sequences:

Cy5-labeled miR-21-hp RNA: 5′-Cy5-GGGUUGACUGUUGAAUCUCAUGGCAACCC-3′ Cy5-labeled TAR RNA: 5′-Cy5-GCAGAUCUGAGCCUGGGAGCUCUCUGCC-3′. miR-21-hp RNA: 5′-GGGUUGACUGUUGAAUCUCAUGGCAACCC-3′. 2-AP-labeled miR-21-hp RNA: 5′-GGGUUGACUGUUGA(2AP)-UCUCAUGGCAACCC-3′

AlexaFluor 647 (NHS Ester)-labeled pre-miR-21-hp RNA: 5′-Alexa647N-UAGCUUAUCAGACUGAUGUUGACUGUUGAAUCUCAUGGCAACACCAGUCGAUG GGCUGUC-3′.

Small Molecule Microarray (SMM) Screening.

SMM slides were prepared according to previously reported procedures.[27,30,31] Briefly, γ-aminopropyl silane (GAPS) microscope slides were functionalized with an Fmoc-protected amino polyethylene glycol spacer (Fmoc-8-amino-3,6-dioxaoctanoic acid) in N,N-dimethylformamide (DMF). Following piperidine deprotection, 1,6-diisocyanatohexane was coupled to the surface to provide isocyanate-functionalized microarray slides for immobilization of small molecule library members containing either primary or secondary alcohols or amines (aliphatic or aromatic). A total of 20 000 unique small molecules (10 mM in DMSO) containing at least one primary or secondary alcohol or amine were purchased from commercial vendors including ChemBridge and ChemDiv. The libraries were printed on four array slides containing ~5000 distinct molecules printed in duplicate, in addition to dyes and controls used for quality control validation. The arrays were exposed to pyridine vapor to facilitate covalent attachment to the isocyanate-functionalized slide surface. Slides were then incubated with a polyethylene glycol solution to quench unreacted isocyanate surface. The deprotected 5′-Cy5-labeled miR-21 hairpin (Cy5-miR-21-hp) from Dharmacon was dissolved in RNase free 1× PBS (12 mM NaH_2PO_4, 137 mM NaCl, 3 mM KCl, pH 7.4) and was annealed by heating to 95 °C for 3 min, followed by slowly cooling to RT for 1 h. The hairpin was then diluted to 500 nM in PBST (0.01% Tween-20) for screening. Printed microarray slides were incubated with the RNA at a concentration of 500 nM for 1 h. Following incubation, slides were washed three times with PBST and once with water to remove unbound RNA, and the slides were dried by centrifugation for 2 min at 4000g. Slides were imaged for fluorescence (650 nm excitation, 670 nm emission) on a GenePix 4000a Microarray Scanner with a resolution of 5 or 10 μm. The scanned image was

aligned with the corresponding GenePix Array List (GAL) file to identify individual features. Hits were determined using the following criteria: (a) coefficient of variance (CV) of duplicate spots < 100, (b) average Z score for a compound > 3, (c) [(Z-score$_{RNAincubated}$) − (Z-score$_{ControlArray}$)]/Z-score$_{ControlArray}$) > 3, (d) no activity with any other nucleic acid structures screened in parallel. Other Cy5-labeled nucleic acids screened in parallel included HIV TAR RNA, the FOXO3 DNA transcription factor binding domain, MYC G4 forming DNA, and CAG DNA repeat, all of which were screened using the same method described above for the miR-21 hairpin. Hits were further validated by visual inspection of array images, and compounds for further study were purchased from original suppliers.

Differential Scanning Fluorimetry.

miR-21-hp RNA from Dharmacon was dissolved in PBS (pH 7.4), annealed by briefly heating to 95 °C for 3 min and cooling to RT for 1 h, and then diluted to 10 μM in PBS. Stock solutions of each small molecule were prepared at a concentration of 1 mM in DMSO. In a white 96-well PCR plate, small molecules were diluted to a final concentration of 30 μM in PBS (50 μL total volume) in triplicate and were incubated with the miR-21-hp RNA at a final concentration of 2 μM for 10 min at RT. SYBR Green II was then added to each well at a final concentration of 2× (5% final DMSO concentration). The solutions were mixed, and the plate was centrifuged at 4000 rpm for 2 min. After a 10 min incubation, the fluorescence was measured on a LightCycler 480 (Roche) as the samples were heated from 20 to 80 °C with a ramp rate of 0.04 °C/s and an acquisition of 10 reads/1 °C using an excitation wavelength of 465 nm and an emission wavelength of 510 nm. The melting temperature (T_m) was determined by the maximum of the negative of the first derivative of the fluorescence vs temperature melting curves. The mean T_m and standard deviations were determined from replicate wells.

2-Aminopurine (2-AP) Fluorescence Titration.

Fluorescence titrations were performed according to previously reported protocols.[23] Deprotected miR-21 hairpin RNA containing a 2-AP label substituted for A15 in the apical loop was purchased from Dharmacon and was dissolved in PBS (pH 7.4) to a concentration of 100 μM. The RNA was annealed by briefly heating to 95 °C for 3 min, followed by cooling to RT for 1 h, and was subsequently diluted to 10 μM in PBS. Small molecule solutions were prepared as serial dilutions in DMSO. In a black 96-well plate, small molecules were diluted to final concentrations ranging from 0.05–500 μM in triplicate in PBS (10% final DMSO concentration), and the miR-21–2AP RNA was added at a final concentration of 2 μM. Background fluorescence of the small molecules was assessed in wells containing compound at each final concentration in PBS in the absence of RNA. After delivery of the RNA, the plate was centrifuged (1000 rpm, 2 min) and allowed to incubate for 30 min at RT with shaking. Fluorescence was then measured on a Synergy Mx microplate reader (BioTek) with an excitation wavelength of 310 nm and an emission wavelength of 365 nm. Background fluorescence of the small molecules in the absence of RNA was subtracted from wells containing RNA, and the apparent dissociation constants were determined by fitting a sigmoidal dose–response curve to the mean fluorescence of background subtracted triplicate measurements.

Fluorescence Intensity Assay.

Fluorescence titrations were performed using a 5′-Cy5-labeled miR-21 hairpin purchased from Dharmacon. The RNA was prepared in 1 × PBS at a concentration of 100 uM and was annealed by heating to 95 °C for 3 min, followed by cooling to RT over 1 h. Small molecule solutions were prepared as serial dilutions in DMSO. In a black 96-well plate, small molecules were diluted to final concentrations ranging from 0 to 250 μM in triplicate in PBS with a 5% final DMSO concentration. After shaking for 5 min, 5′Cy5-miR-21-hp RNA was added to a final concentration of 100 nM. The samples were allowed to equilibrate for 30 min with shaking. The fluorescence intensity was then measured on a Synergy Mx microplate reader (BioTek) at an excitation wavelength of 649 nm and an emission wavelength of 670 nm. The fluorescence intensity was then normalized to the values obtained for RNA incubated with a DMSO control and was plotted against small molecule concentration. The apparent dissociation constants were determined using a single site model to fit the curve.

Inhibition of Dicer Cleavage.

Dicer cleavage assays were performed on 5′-AlexaFluor 647-labeled pre-miR-21-hp RNA and were monitored by the presence of full length RNA.[40] 5′-AlexaFluor 647-labeled pre-miR-21 was dissolved in PBS (pH 7.4) to a concentration of 100 μM and was annealed by briefly heating to 95 °C for 3 min, followed by slowly cooling to RT over 1 h. For assessing each compound at a single concentration, the annealed RNA was preincubated at a final concentration of 10 nM in 20 mM Tris at pH 7.4, 12 mM NaCl, 2.5 mM MgCl$_2$, 40 U/mL RNaseOUT (Invitrogen), and 1.0 mM fresh DTT with either a DMSO control (5% final concentration) or each compound at a concentration of 1 μM at RT for 30 min. Recombinant Dicer (0.05 U, Genlantis) was then added, and digestion was performed at 37 °C for 2 h. Digestions were quenched by adding an equal volume of 2× TBE/urea sample buffer (BioRad) and heating to 95 °C for 5 min. Cleavage was analyzed using a 15% TBE/Urea polyacrylamide gel and was visualized by fluorescence of the 5′-Alexa Fluor 647 label (630 nm excitation, 670 emission) with an ImageQuant LAS 4000 gel imager (GE Healthcare Life Sciences), and the background-corrected fluorescence intensity of the full length RNA was analyzed using ImageQuant software. The fluorescence intensity for full length RNA in the small molecule treated samples was normalized to DMSO controls with and without Dicer within the same experiment. Digestions were performed in triplicate on separate days, and the normalized fluorescence for each compound was averaged and standard deviations were determined. For the dose–response experiment, the annealed RNA was preincubated at a final concentration of 500 nM in 20 mM Tris at pH 7.4, 12 mM NaCl, 2.5 mM MgCl$_2$, 40 U/mL RNaseOUT (Invitrogen), and 1.0 mM fresh DTT with either a DMSO control (5% final concentration) or small molecule at concentrations ranging from 0.1 to 100 μM at RT for 30 min. Recombinant Dicer (0.5 U) was then added, and digestion was performed at 37 °C for 30 min. Digestions were analyzed using a 15% TBE/urea polyacrylamide gel and visualized as described previously.

Analysis of Mg²⁺-Induced In-line Cleavage.

5′-Cy5-labeled miR-21-hp RNA was dissolved in $0.1 \times$ PBS (pH 7.4) to a concentration of 100 μM and was annealed by briefly heating to 95 °C for 3 min, followed by slowly cooling to RT for 1 h.[22,23] The annealed RNA was incubated at a final concentration of 3 μM in 50 mM Tris at pH 8.5, 10 mM KCl buffer with either a DMSO control (5% final concentration), or compound at a concentration of 3, 10, 30, 100, or 300 μM. MgCl₂ was added at a final concentration of 1 mM, and the reactions were incubated at RT in darkness for 4 days. Alkaline hydrolysis was performed in 10 mM NaHCO₃ at pH 9.0 and 95 °C for 5 min. Ribonuclease T1 digestion was carried out with 0.1 U of ribonuclease T1 (Ambion) in 20 mM Tris at pH 7.5, 50 mM NaCl, and 0.1 mM MgCl₂ at RT for 20 min. The RNase T1 reaction was stopped by adding 0.2 volumes of 5 mM EDTA. Equal volumes of loading buffer containing 7 M urea, $1 \times$ TBE, and 0.01% direct red dye was added to each reaction, and the samples were heated to 95 °C for 5 min prior to analysis by electrophoresis on a denaturing polyacrylamide sequencing gel (20%, 19:1 cross-linking, 7 M urea). The gel was visualized by fluorescence of the 5′-Cy5 label (630 nm excitation, 670 emission) with a Typhoon FLA9500 gel imager (GE Healthcare Life Sciences) and was analyzed with ImageQuant software.

Supplementary Material

Refer to Web version on PubMed Central for supplementary material.

ACKNOWLEDGMENTS

REFERENCES

(1). Thomas JR, and Hergenrother PJ (2008) Targeting RNA with small molecules. Chem. Rev 108, 1171–1224. [PubMed: 18361529]

(2). Guan LR, and Disney MD (2012) Recent Advances in Developing Small Molecules Targeting RNA. ACS Chem. Biol 7, 73–86. [PubMed: 22185671]

(3). Connelly CM, Moon MH, and Schneekloth JS, Jr. (2016) The Emerging Role of RNA as a Therapeutic Target for Small Molecules. Cell Chem. Biol 23, 1077–1090. [PubMed: 27593111]

(4). Le Grice SF (2015) Targeting the HIV RNA genome: high-hanging fruit only needs a longer ladder. Curr. Top. Microbiol. Immunol 389, 147–169. [PubMed: 25735922]

(5). Breaker RR, and Joyce GF (2014) The expanding view of RNA and DNA function. Chem. Biol 21, 1059–1065. [PubMed: 25237854]

(6). Hayes J, Peruzzi PP, and Lawler S (2014) MicroRNAs in cancer: biomarkers, functions and therapy. Trends Mol. Med 20, 460–469. [PubMed: 25027972]

(7). Sahu A, Singhal U, and Chinnaiyan AM (2015) Long noncoding RNAs in cancer: from function to translation. Trends Cancer 1, 93–109. [PubMed: 26693181]

(8). Cheetham SW, Gruhl F, Mattick JS, and Dinger ME (2013) Long noncoding RNAs and the genetics of cancer. Br. J. Cancer 108, 2419–2425. [PubMed: 23660942]

(9). Ameres SL, and Zamore PD (2013) Diversifying microRNA sequence and function. Nat. Rev. Mol. Cell Biol. 14, 475–488. [PubMed: 23800994]

(10). Li S, Liang Z, Xu L, and Zou FD (2012) MicroRNA-21: a ubiquitously expressed pro-survival factor in cancer and other diseases. Mol. Cell. Biochem 360, 147–158. [PubMed: 21909994]

(11). Jazbutyte V, and Thum T (2010) MicroRNA-21: From Cancer to Cardiovascular Disease. Curr. Drug Targets 11, 926–935. [PubMed: 20415649]

(12). Medina PP, Nolde M, and Slack FJ (2010) OncomiR addiction in an in vivo model of microRNA-21-induced pre-B-cell lymphoma. Nature 467, 86–90. [PubMed: 20693987]

(13). Zhou X, Ren Y, Moore L, Mei M, You Y, Xu P, Wang B, Wang G, Jia Z, Pu P, Zhang W, and Kang C (2010) Downregulation of miR-21 inhibits EGFR pathway and suppresses the growth of human glioblastoma cells independent of PTEN status. Lab. Invest 90, 144–155. [PubMed: 20048743]

(14). Gabriely G, Wurdinger T, Kesari S, Esau CC, Burchard J, Linsley PS, and Krichevsky AM (2008) MicroRNA 21 promotes glioma invasion by targeting matrix metalloproteinase regulators. Mol. Cell. Biol 28, 5369–5380. [PubMed: 18591254]

(15). Si ML, Zhu S, Wu H, Lu Z, Wu F, and Mo YY (2007) miR-21-mediated tumor growth. Oncogene 26, 2799–2803. [PubMed: 17072344]

(16). Meng F, Henson R, Wehbe-Janek H, Ghoshal K, Jacob ST, and Patel T (2007) MicroRNA-21 regulates expression of the PTEN tumor suppressor gene in human hepatocellular cancer. Gastroenterology 133, 647–658. [PubMed: 17681183]

(17). Wagenaar TR, Zabludoff S, Ahn SM, Allerson C, Arlt H, Baffa R, Cao H, Davis S, Garcia-Echeverria C, Gaur R, Huang SM, Jiang L, Kim D, Metz-Weidmann C, Pavlicek A, Pollard J, Reeves J, Rocnik JL, Scheidler S, Shi C, Sun F, Tolstykh T, Weber W, Winter C, Yu E, Yu Q, Zheng G, and Wiederschain D (2015) Anti-miR-21 Suppresses Hepatocellular Carcinoma Growth via Broad Transcriptional Network Deregulation. Mol. Cancer Res. 13, 1009–1021. [PubMed: 25758165]

(18). Naro Y, Thomas M, Stephens MD, Connelly CM, and Deiters A (2015) Aryl amide small-molecule inhibitors of microRNA miR-21 function. Bioorg. Med. Chem. Lett 25, 4793–4796. [PubMed: 26220158]

(19). Gumireddy K, Young DD, Xiong X, Hogenesch JB, Huang Q, and Deiters A (2008) Small-molecule inhibitors of microrna miR-21 function. Angew. Chem., Int. Ed 47, 7482–7484.

(20). Bose D, Jayaraj G, Suryawanshi H, Agarwala P, Pore SK, Banerjee R, and Maiti S (2012) The tuberculosis drug streptomycin as a potential cancer therapeutic: inhibition of miR-21 function by directly targeting its precursor. Angew. Chem., Int. Ed 51, 1019–1023.

(21). Chen Y, Yang F, Zubovic L, Pavelitz T, Yang W, Godin K, Walker M, Zheng S, Macchi P, and Varani G (2016) Targeted inhibition of oncogenic miR-21 maturation with designed RNA-binding proteins. Nat. Chem. Biol 12, 717–723. [PubMed: 27428511]

(22). Diaz JP, Chirayil R, Chirayil S, Tom M, Head KJ, and Luebke KJ (2014) Association of a peptoid ligand with the apical loop of pri-miR-21 inhibits cleavage by Drosha. RNA 20, 528–539. [PubMed: 24497550]

(23). Chirayil S, Chirayil R, and Luebke KJ (2009) Discovering ligands for a microRNA precursor with peptoid microarrays. Nucleic Acids Res. 37, 5486–5497. [PubMed: 19561197]

(24). Hong JA, Neel DV, Wassaf D, Caballero F, and Koehler AN (2014) Recent discoveries and applications involving small-molecule microarrays. Curr. Opin. Chem. Biol 18, 21–28. [PubMed: 24534749]

(25). Wu H, Ge J, Uttamchandani M, and Yao SQ (2011) Small molecule microarrays: the first decade and beyond. Chem. Commun. (Cambridge, U. K.) 47, 5664–5670.

(26). Duffner JL, Clemons PA, and Koehler AN (2007) A pipeline for ligand discovery using small-molecule microarrays. Curr. Opin. Chem. Biol 11, 74–82. [PubMed: 17169601]

(27). Bradner JE, McPherson OM, and Koehler AN (2006) A method for the covalent capture and screening of diverse small molecules in a microarray format. Nat. Protoc 1, 2344–2352. [PubMed: 17406478]

(28). Bryan MC, and Wong CH (2004) Aminoglycoside array for the high-throughput analysis of small molecule-RNA interactions. Tetrahedron Lett. 45, 3639–3642.

Author Manuscript Author Manuscript Author Manuscript Author Manuscript

(29). Childs-Disney JL, Wu ML, Pushechnikov A, Aminova O, and Disney MD (2007) A small molecule microarray platform to select RNA internal loop-ligand interactions. ACS Chem. Biol 2, 745–754. [PubMed: 17975888]

(30). Felsenstein KM, Saunders LB, Simmons JK, Leon E, Calabrese DR, Zhang S, Michalowski A, Gareiss P, Mock BA, and Schneekloth JS, Jr. (2015) Small Molecule Microarrays Enable the Identification of a Selective, Quadruplex-Binding Inhibitor of MYC Expression. ACS Chem. Biol 11, 139. [PubMed: 26462961]

(31). Sztuba-Solinska J, Shenoy SR, Gareiss P, Krumpe LR, Le Grice SF, O'Keefe BR, and Schneekloth JS, Jr. (2014) Identification of biologically active, HIV TAR RNA-binding small molecules using small molecule microarrays. J. Am. Chem. Soc 136, 8402–8410. [PubMed: 24820959]

(32). MacMillan KS, Naidoo J, Liang J, Melito L, Williams NS, Morlock L, Huntington PJ, Estill SJ, Longgood J, Becker GL, McKnight SL, Pieper AA, De Brabander JK, and Ready JM (2011) Development of proneurogenic, neuroprotective small molecules. J. Am. Chem. Soc 133, 1428–1437. [PubMed: 21210688]

(33). Naidoo J, De Jesus-Cortes H, Huntington P, Estill S, Morlock LK, Starwalt R, Mangano TJ, Williams NS, Pieper AA, and Ready JM (2014) Discovery of a neuroprotective chemical, (S)-N-(3-(3,6-dibromo-9H-carbazol-9-yl)-2-fluoropropyl)-6-methoxypyridin-2-amine [(−)-P7C3-S243], with improved druglike properties. J. Med. Chem 57, 3746–3754. [PubMed: 24697290]

(34). Van Gelder JM, Basel Y, Kraiz BO, Mouallem O, Miron D, Gur-Arie N, and Klein J Heparanase inhibitors and uses thereof. U.S. Patent Application 2007185176. 8 9, 2007.

(35). Gelder JV, Basel Y, Kraiz B, Mouallem O, Miron D, Gur-Arie N, and Klein J Heparanase inhibitors and uses thereof, US Patent No US20070185176 A1, Feb. 6, 2004.

(36). Soukup GA, and Breaker RR (1999) Relationship between internucleotide linkage geometry and the stability of RNA. RNA 5, 1308–1325. [PubMed: 10573122]

(37). Pieper AA, Xie S, Capota E, Estill SJ, Zhong J, Long JM, Becker GL, Huntington P, Goldman SE, Shen CH, Capota M, Britt JK, Kotti T, Ure K, Brat DJ, Williams NS, MacMillan KS, Naidoo J, Melito L, Hsieh J, De Brabander J, Ready JM, and McKnight SL (2010) Discovery of a proneurogenic, neuroprotective chemical. Cell 142, 39–51. [PubMed: 20603013]

(38). Wang G, Han T, Nijhawan D, Theodoropoulos P, Naidoo J, Yadavalli S, Mirzaei H, Pieper AA, Ready JM, and McKnight SL (2014) P7C3 neuroprotective chemicals function by activating the rate-limiting enzyme in NAD salvage. Cell 158, 1324–1334. [PubMed: 25215490]

(39). Frye SV (2010) The art of the chemical probe. Nat. Chem. Biol 6, 159–161. [PubMed: 20154659]

(40). Lorenz DA, Song JM, and Garner AL (2015) High-throughput platform assay technology for the discovery of premicrorna-selective small molecule probes. Bioconjugate Chem. 26, 19–23.
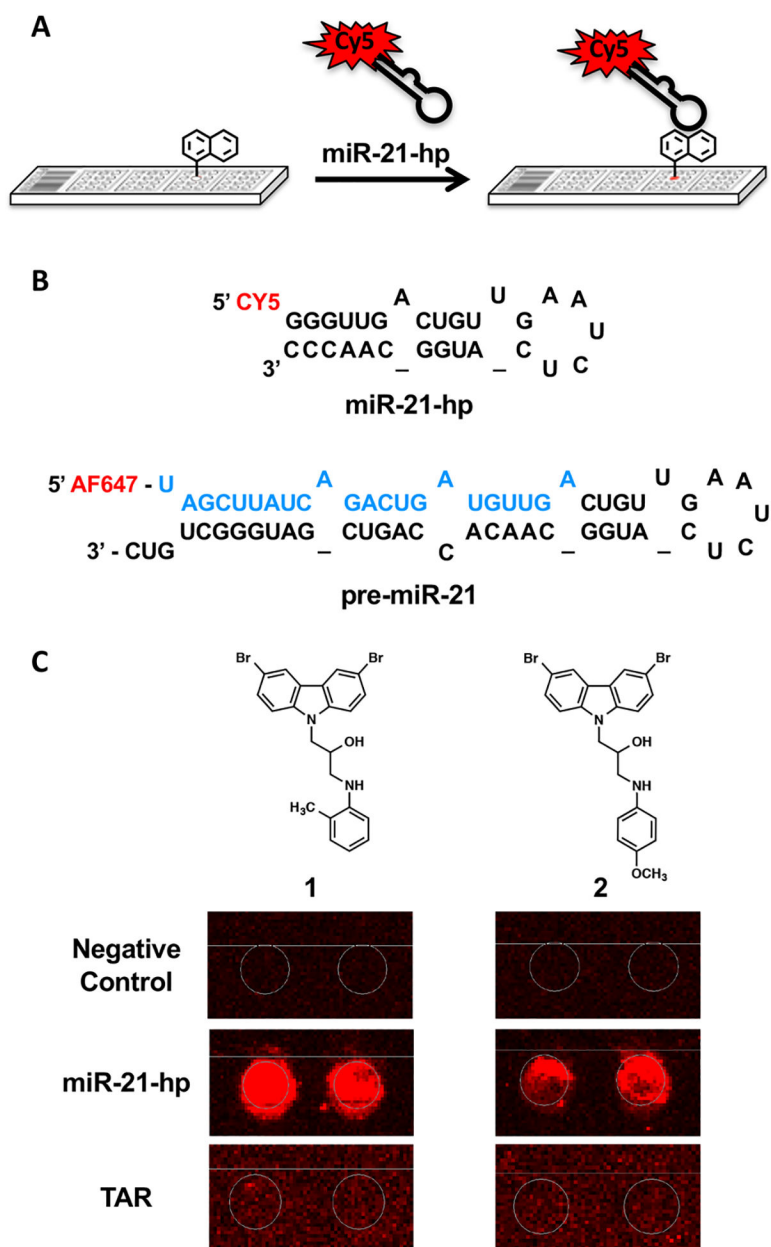
Figure 1.
Small molecule microarray screening. (A) Cartoon depicting a small molecule microarray screen to identify compounds that bind to miR-21-hp RNA. (B) Sequence of the truncated Cy5-labeled miR-21 hairpin used in the SMM screening and subsequent in-line probing (top) and full length AlexaFluor 647-labeled precursor miR-21 (premiR-21) used in the Dicer cleavage assays (bottom). The sequence of mature miR-21 is indicated in blue. (C) Raw SMM images for hit structures (compounds are printed in duplicate). The behavior of each compound in the negative control (buffer) incubated, Cy5-labeled miR-21-hp RNA incubated, and Cy5-labeled HIV TAR hairpin RNA incubated SMMs are shown for comparison.
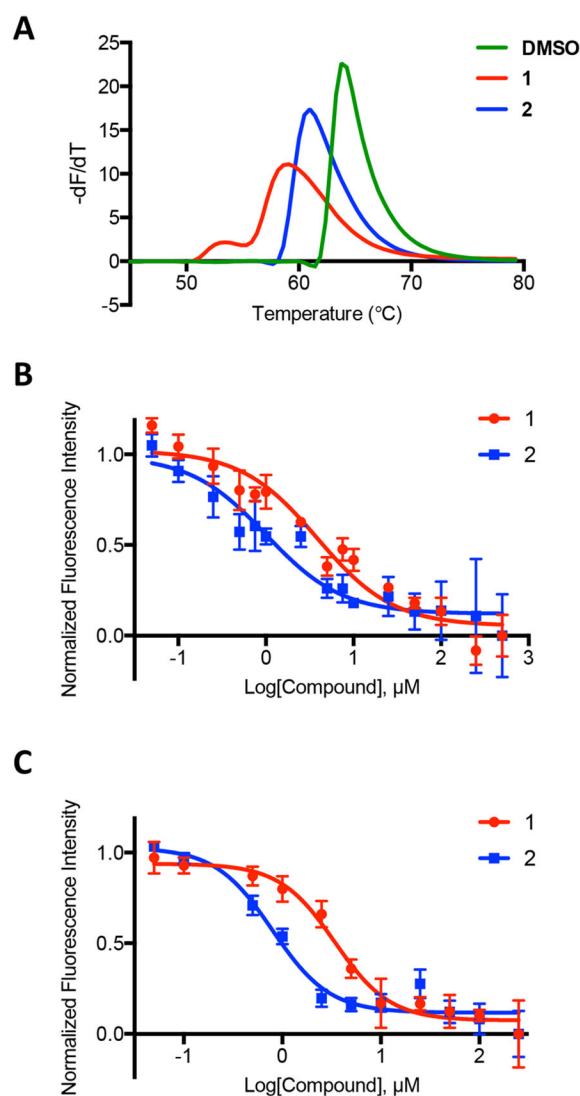
Figure 2.
Validation of hit compounds identified by SMM screening. (A) Differential scanning
fluorimetry (DSF) experiments demonstrating changes in the melting temperature (Tm) of
the unlabeled miR-21-hp RNA upon addition of **1** or **2** at 30 μM in triplicate compared to a
DMSO control. (B) 2-Aminopurine fluorescence titration of 2-AP-labeled miR-21-hp RNA
in the presence of **1** or **2** at increasing concentrations. (C) Fluorescence titration assay of 5′-
Cy5-labeled miR-21-hp RNA in the presence of increasing concentration of **1** or **2**. Apparent
K_d values for each compound were determined from triplicate experiments using both the 2-
AP and fluorescence titration assays. The error bars indicate the standard deviation
determined from three independent measurements.
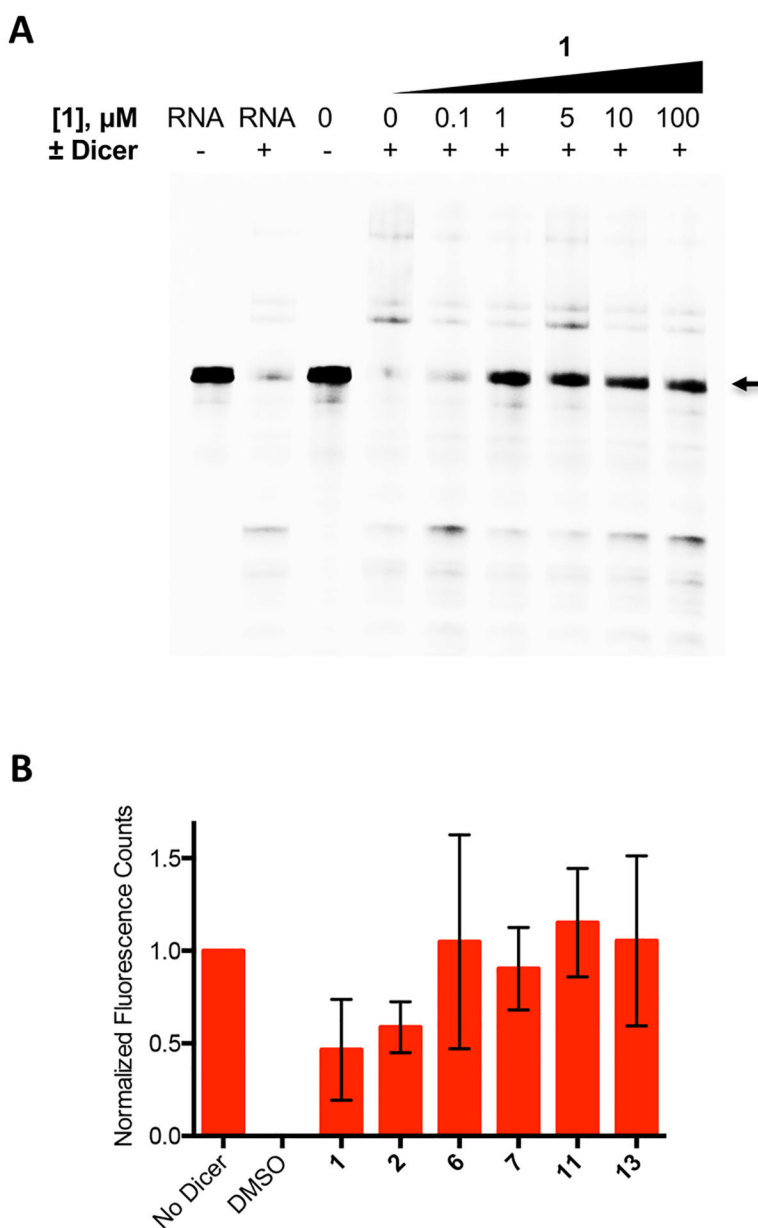
Figure 3.
Dicer cleavage assays of full length 5′-AlexaFluor 647-labeled pre-miR-21. (A) In-gel fluorescence of 5′-AlexaFluor 647-labeled premiR-21 cleaved with Dicer in the presence of increasing concentration of **1**. Arrow indicates the band corresponding to the unprocessed premiR-21, which was used for quantitation. (B) Quantification of in-gel fluorescence of 5′-AlexaFluor647-labeled pre-miR-21 in the presence of Dicer and the miR-21 binding compounds at a concentration of 1 μM. Treatments were performed in triplicate, and compound treatment was normalized to DMSO controls with and without Dicer within the same experiment. The error bars indicate the standard deviation determined from the three independent experiments.
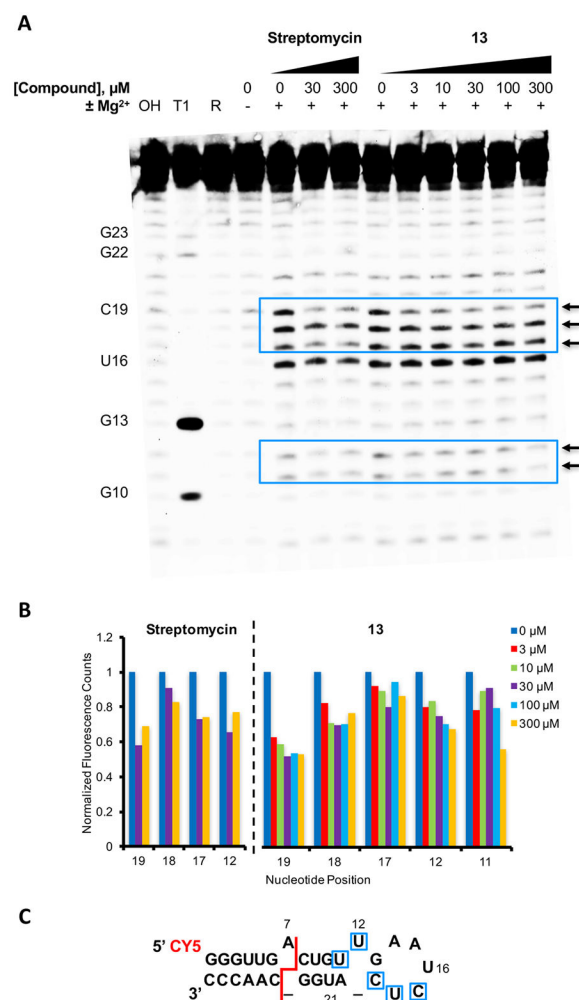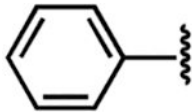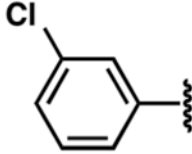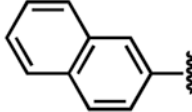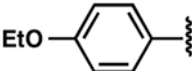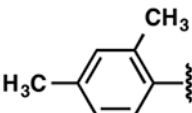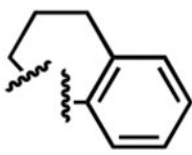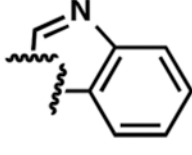
Figure 4.
Analysis of small molecule binding to miR-21-hp RNA by Mg^{2+} induced in-line cleavage.
(A) In-gel fluorescence of 5′-Cy5-labeled miR-21-hp RNA after treatment with **13** at concentrations of 3, 10, 30, 100, or 300 μM or a DMSO control in the absence (−) or presence (+) of 1 mM MgCl$_2$. OH and T1 are a partial alkaline hydrolysis ladder and ribonuclease T1 digestion, respectively. Arrows designate nucleotide positions where the cleavage efficiency was significantly altered by compound treatment. (B) Quantification of fluorescent band intensity from above gel, where band intensity from **13** or streptomycin treated samples was normalized to the average band intensity of DMSO control treated samples. (C) Structure of the 5′-Cy5-labeled miR-21-hp RNA used for the in-line probing. Significant changes to the cleavage pattern in the presence of small molecule are indicated in blue. The red line indicates the putative Dicer cleavage site on pre-miR-21.

Table 1.

Synthesis and Evaluation of Aniline Modified Analogs of 1 and 2[c]
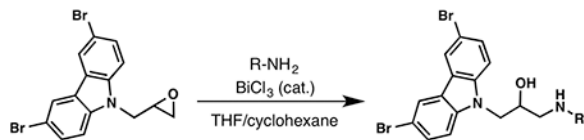
Compound	R-NH$_2$	T$_m$ (°C)	FIA K_d (μM)	2-AP K_d(μM)
1		−5.1 ± 1.9	3.2 ± 0.7	2.3 ± 0.5
2		−2.3 ± 0.3	0.7 ± 0.1	0.8 ± 0.2
3		−1.2 ± 0.2	3.0 ± 0.6	3.2 ± 0.5
4		−2.2 ± 0.6	1.4 ± 0.3	2.7 ± 0.3
5		−1.6 ± 0.4	4.8 ± 1.0	7.4 ± 1.9
6		−3.7 ± 0.1	2.2 ± 0.3	4.8 ± 1.4
7		−1.0 ± 0.3	2.1 ± 0.5	2.9 ± 0.5
8		−1.6 ± 0.5	3.3 ± 1.6	3.2 ± 0.7
9		−4.7 ± 0.4	2.9 ± 0.9	15.5 ± 5.5

Compound	R-NH$_2$	T$_m$ (°C)	FIA K_d (μM)	2-AP K_d(μM)
10		−5.5 ± 1.9	2.1 ± 0.9	3.2 ± 0.7
11[a]		−9.3 ± 1.9[b]	1.4 ± 0.4	1.2 ± 0.2
12[a]		−6.6 ± 2.2	1.4 ± 0.5	0.8 ± 0.3
13		−4.5 ± 0.2	1.2 ± 0.3	2.0 ± 0.6
14		−2.7 ± 0.6	11.3 ± 4.4	5.1 ± 3.0
15		−0.4 ± 0.2	3.4 ± 1.7	5.1 ± 2.5
16[a]		−5.5 ± 1.9	2.3 ± 0.5	4.0 ± 1.2

[a]Compound showed poor solubility at higher concentrations.
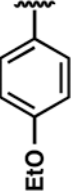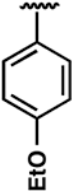
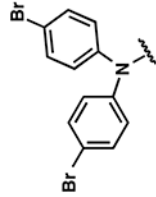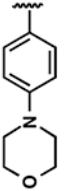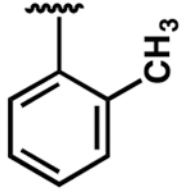[b]Compound displayed broad T_m curve.
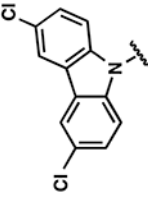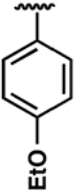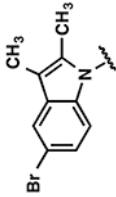
[c]The T_m and apparent K_d values were determined by differential scanning fluorimetry, 2-aminopurine, and fluorescence intensity assays.

Table 2.

Synthesis and Evaluation of Carbazole Modified Analogs of 1 and 2[a]
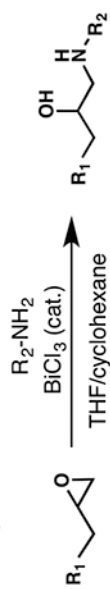
Compound	R₁	R₂-NH₂	T_m (°C)	FIA K_d (μM)	2-AP K_d (μM)
17			-0.5 ± 0.2	9.2 ± 2.4	8.3 ± 0.1
18		EtO	-4.7 ± 0.1	2.2 ± 0.5	2.0 ± 0.3
19			-1.4 ± 0.6	4.6 ± 1.3	3.2 ± 0.6
20		EtO	-0.7 ± 0.8	1.4 ± 0.6	1.0 ± 0.3
21			-0.1 ± 0.8	9.2 ± 2.6	2.1 ± 0.4
22		CH₃	-1.1 ± 0.7	3.8 ± 0.5	2.7 ± 1.1

Compound	R$_1$	R$_2$-NH$_2$	T$_m$ (°C)	FIA K_d (μM)	2-AP K_d (μM)
23			−2.2 ± 0.8	3.2 ± 0.8	3.7 ± 1.3
24			−2.1 ± 0.4	>10	>10
25			−1.7 ± 0.7	2.3 ± 0.6	4.2 ± 0.8
26			−1.2 ± 0.3	>10	3.6 ± 0.6
27			−1.0 ± 0.6	>10	4.4 ± 0.8

[a]The T_m and apparent K_d values were determined by differential scanning fluorimetry, 2-aminopurine, and fluorescence intensity assays.